Supporting Information

Mechanically Viscoelastic Properties of Cellulose Nanocrystals Skeleton in Hierarchical Composite Hydrogels

Jun Yang*, ChunRui Han

Beijing Key Laboratory of Lignocellulosic Chemistry, Beijing Forestry University, Beijing, 100083, China

* Correspondent author: yangjun11@bjfu.edu.cn

Contents

Table S1 Mechanical properties summary of composite hydrogels

Figure S1 CNC skeleton density and porosity as a function of CNC concentration

Figure S2 Compressive curves of CNC skeleton

Figure S3 Image of the composite hydrogels stability

Figure S4 FTIR and TGA curves of gels

Figure S5 DSC curves the composite hydrogels

Figure S6 Skeleton strategy vs. randomly distributed CNC in mechanical properties

Description of Cryo-SEM and ultramicrotoming for TEM

Calculation of hardness and modulus in nanoindentation measurement

Table S1 Mechanical properties of the composite hydrogels with different volume fractions of CNC

Sample	CNC fraction (vol%)	Maximum tensile strength (kPa)	Elongation at break (%)	Young's modulus (kPa)	Toughness[a)] (kJ/m^3)	Compressive strength (kPa at 90% strain)	Fracture energy (kJ/m^2)
CNC0.2	0.2	73 ± 2.7	647 ± 25	11.4 ± 0.34	6.7 ± 0.17	165 ± 2.2	1.22 ± 0.13
CNC0.5	0.5	115 ± 3.1	957 ± 34	16.8 ± 0.51	9.5 ± 0.23	348 ± 2.6	1.56 ± 0.16
CNC1	1	151 ± 3.2	1392 ± 51	22.2 ± 0.63	13 ± 0.26	510 ± 3.1	2.01 ± 0.18
CNC1.5	1.5	173 ± 3.3	1247 ± 46	26.5 ± 0.74	17 ± 0.3	647 ± 3.4	2.49 ± 0.21
CNC2	2	181 ± 3.5	1021 ± 39	29.8 ± 0.84	21 ± 0.32	1017 ± 4.1	2.82 ± 0.22
PAAm	-	35 ± 1.7	450 ± 11	7.3 ± 0.15	3.3 ± 0.11	92 ±1.8	0.14 ± 0.02

[a)]The toughness was calculated from the area under the tensile stress-strain curves.

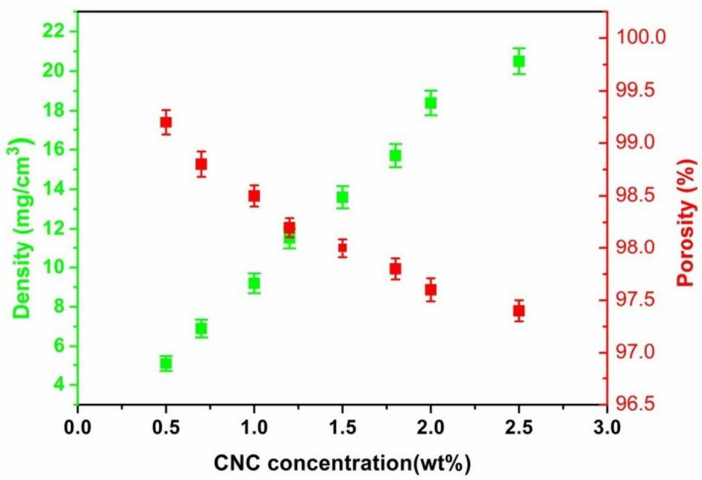

Figure S1. The density and porosity of CNC skeleton as a function of initial suspension concentration by freeze drying procedure.

CNC skeleton densities were calculated by measuring the weight and volume of each individual aerogel. The weight of a specimen was measured by an analytical balance and the dimensions of the specime were measured by a digital caliper at four different positions. Six independent data for each specimen were recorded to calculate the average values and errors. For porosity (P), it can be determined by following equation: [1]

$$P(\%) = 100 \times (1 - \rho_{Skeleton}/\rho_{CNC})$$

where $\rho_{Skeleton}$ and ρ_{CNC} are density of the skeleton and density of cellulose nanocrystals, respectively (assuming the gas density was negligible).

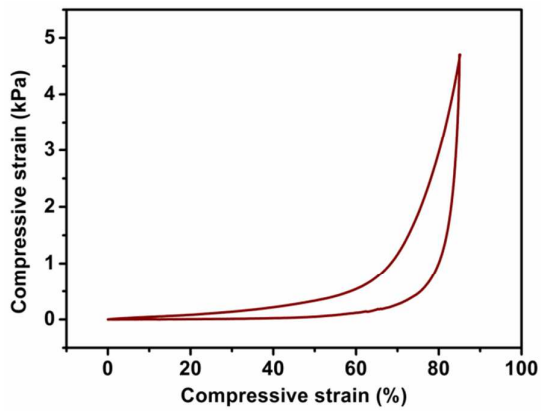

Figure S2. Compressive loading-unloading curves of CNC template (initial CNC concentration 1.5 wt%).

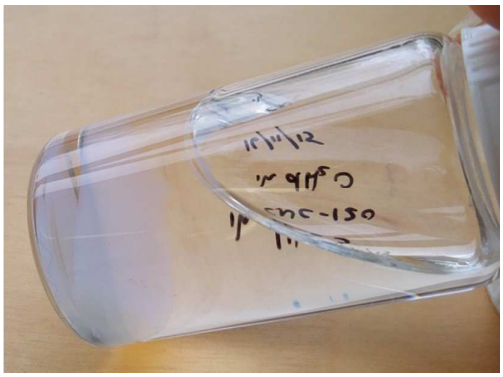

Figure S3. Image of CNC skeleton reinforced composite hydrogels during in-situ polymerization (t = 50 min) and reveals structural integrity, inferring the growth of polymer chains does not lead to dissociation of CNC skeleton.

FTIR and thermal analysis

IR spectra of the samples were recorded using Perkin Elmer FT-IR Spectra 2000 at room temperature (25 °C).The test specimens were prepared using the KBr disc method and analyzed over the range of 400–4000 cm^{-1}. Thermogravimetric analyses (TGA) were conducted with Shimadzu DTG (TA-60), heating samples from ambient temperature to 800 °C at the heating rate of 10 °C min^{-1} in a nitrogen atmosphere.

PAM spectra exhibited distinct peaks at 3421 and 3215 cm^{-1}, representing N–H asymmetric and symmetric stretching vibrations at 1658 and 1451 cm^{-1}, which corresponded to the C=O stretching of the amide I band and C–N stretching, respectively. For composite gels (CNC1), C=O stretching in the composites shifted the lower wavenumber and there shows some new peaks at 3617, 3725 and 3861 cm^{-1}, inferring the existence of hydrogen bonds between oxygen-containing groups of CNC and N-H bonds of PAM. For TGA curves, the thermal stability of composite gels is higher

pristine PAAm gels, which is consistent with the interfacial interactions between CNC and PAAm favor the cross-linked network structure.

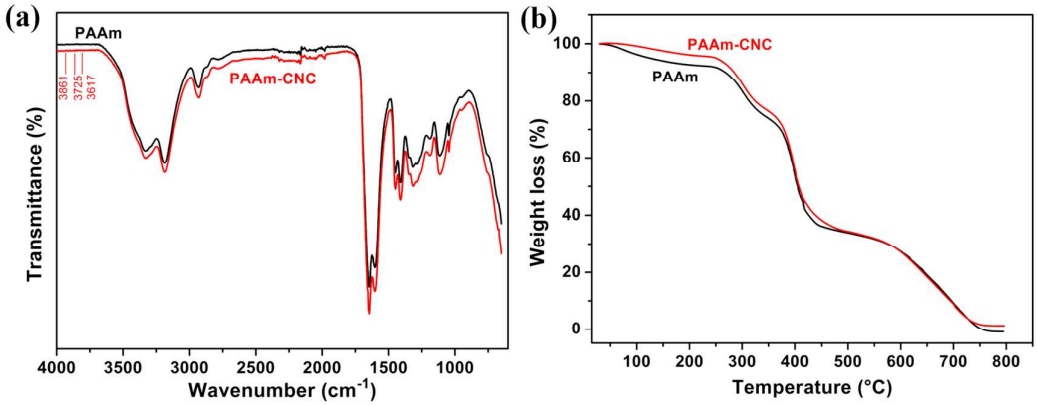

Figure S4. (a) FTIR spectra and (b) TGA curves of PAAm and CNC1 composite gels.

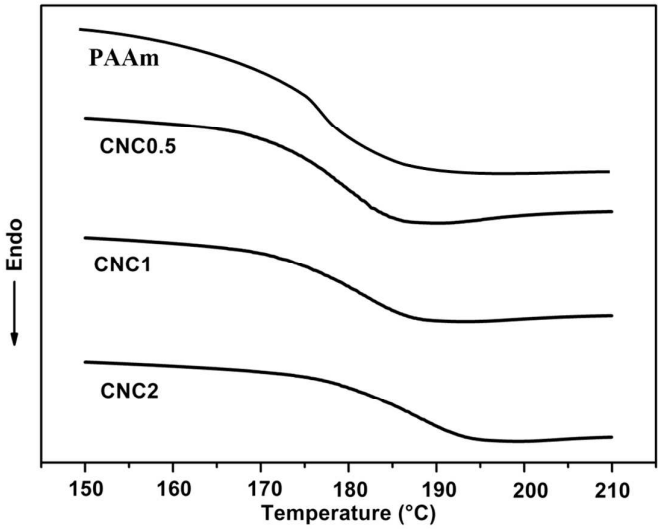

Figure S5. DSC curves show the increased T_g with increasing CNC skeleton fraction, suggesting the confinement effect on the mobility of PAM chains.

Thermal analysis was carried out using a Q10 differential scanning calorimeter manufactured by TA Instruments calibrated with an indium standard. The DSC cell was purged with dry nitrogen flowing at a rate of 20 mL/min. The freeze-dried samples were heated from ambient temperature to 220 °C at a rate of 10 °C /min.

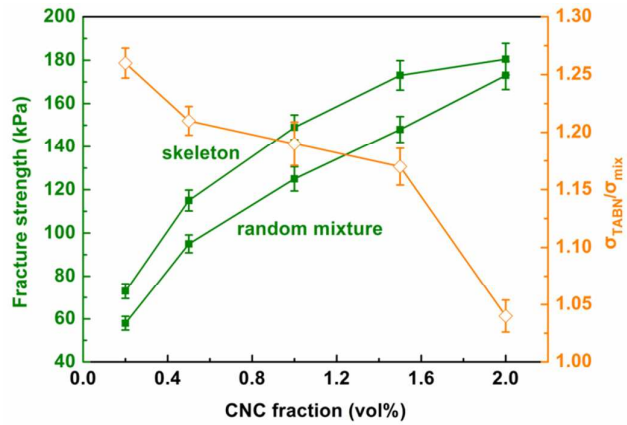

Figure S6. Tensile properties of CNC reinforced hydrogels prepared by skeleton strategy vs. random mixture method. The right *y*-axis indicates the reinforcement ratio by fracture strength of the composite hydrogels over that of random mixture at the same CNC loading.

Cryo-Scanning Electron Microscopy (Cryo-SEM)

The hybrid gels were uniaxially stretched and "fixed" with tape, then cryo-fractured by immersing into liquid nitrogen, and then cut with a cold scalpel. The frozen and cut samples were sublimated at −90 °C for 5 min, followed by sputter coating with platinum at −130 °C for 20 s. Then coated samples were observed with a DSM 960 Zeiss SEM at −140 °C.

The small piece of dried gels were placed in a mold with cubic shape (~1 cm^3), and a hardening resin was added to the mold that the samples kept its position in the approximate middle of the resin. Then the mold with embedded sample was dried in an air-circulation oven for 48 h to obtain the dried samples in hard resin. The gel sample was fixed into the slice cutting machine, where the cross section of samples was sectioned at 90° relative to the surface (minimize the distortion of the structure) using a Leica Ultracut-E microtome that equipped with a diamond knife. The approximately 100 nm thick sections were collected, stained on a carbon support gird, and then observed by JEM-1010 (JEOL).

Nanoindentation Measurement

Hardness (H) is defined as the indentation load divided by the projected area of the indentation, and can be calculated from the load-displacement curves:

$$H = \frac{P_{\max}}{A}$$

where A is the projected contact area. For a given indenter (Berkovich tip in this work), the projected contact area is a function of contact depth.

The elastic modulus was calculate by fitting the unloading curve to a powder law relation (Oliver-Pharr equation[2]), and the slope of the initial part of the unloading curve gives the stiffness (S)

$$S = \frac{dp}{dh}$$

where p is the applied load and h is the displacement. According to Sneddon et al.,[3] the indentation of an elastic half space by any punch can be described as a solid of revolution of a smooth function, a geometry becomes independent with contact stiffness, contact area. Thus, the elastic modulus can be derived by following equation

$$S = 2\beta\sqrt{\frac{A}{\pi}}E_r$$

where β is a constant depending on tip geometry (β =1.034 for Berkovich indenter), A is the projected area of indentation. For a Berkovich indenter, the relation between A and the depth h can is given by

$$A = 24.5 \times h^2$$

The elastic modulus E_r is defined by

$$\frac{1}{E_r} = \left(\frac{1-\upsilon^2}{E}\right)_{\text{specimen}} + \left(\frac{1\text{-}\upsilon_i^{\,2}}{E_i}\right)_{indenter}$$

The contribution of elastic modulus comes from the specimen, with elastic modulus E and Poisson's ratio, v, and the indenter, with elastic modulus and Poisson's ratio of E_i (1140 GPa) and v_i (0.07), respectively.

According to Briscoe et al.,[4] the plasticity index (χ), a parameter to characterize the relative plastic/elastic behavior of the material when it undergoes external stress, was determined as follows:

$$\chi = \frac{A_1}{A_1 + A_2}$$

where A_1 is the area encompassed between the loading and unloading curves (corresponds to the plastic work dome during the indentation), and A_2 is the area encompassed by the unloading curve (corresponds to viscoelastic recovery). Thus, it follows $\chi = 0$ (A_1=0) for an ideal elastic deformation, $0<\chi<1$ for a viscoelastic deformation, and $\chi = 1$ (A_2=0) for an ideal plastic deformation.

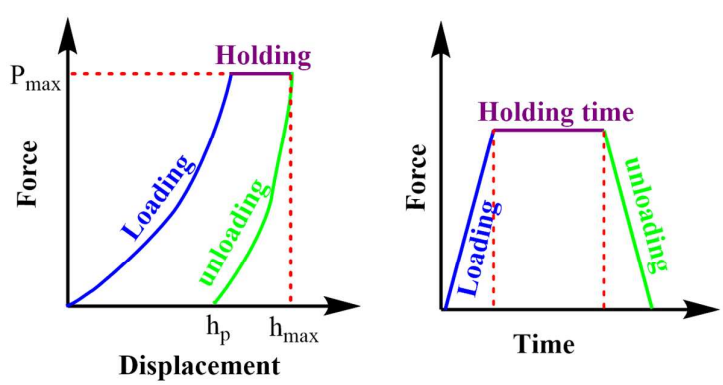

Figure S7. Schematic illustration of a typical force-displacement of a nanoindentation test. P_{max} = maximum load force, h_{max} = maximum penetration depth, h_f = permanent penetration depth

References

(1) Yang, X.; Cranston, E. D. Chem. Mater. 2014, 26, 6016−6025.

(2) Oliver W.C., Pharr G.M. J. Mate. Res.1992, 7, 1564-1583.

(3) Sneddon, Ian N. Int. J. Eng. Sci. 1965, 3, 47–56.

(4) Briscoe, B. J.; Fiori, L.; Pelillo, E. Phys. D: Appl. Phys. 1998, 31, 2395−2405.